Tectonophysics 472 (2009) 290–300

Contents lists available at ScienceDirect

Tectonophysics

journal homepage: www.elsevier.com/locate/tecto

A proposal for a standard procedure of modeling 3-D velocity structures and its application to the Tokyo metropolitan area, Japan

Kazuki Koketsu [a,*], Hiroe Miyake [a], Afnimar [b,1], Yasuhisa Tanaka [a]

[a] Earthquake Research Institute, University of Tokyo, 1-1-1 Yayoi, Bunkyo-ku, Tokyo 113-0032, Japan
[b] Department of Geophysics and Meteorology, Bandung Institute of Technology, Bandung, Indonesia

ARTICLE INFO

Article history:
Received 21 March 2007
Received in revised form 3 May 2008
Accepted 26 May 2008
Available online 8 June 2008

Keywords:
3-D velocity structure
Sedimentary basin
Modeling procedure
Joint inversion
Ground motion simulation
Tokyo metropolitan area

ABSTRACT

Most metropolitan areas are located over large-scale sedimentary basins. Since the sediments filling basins amplify ground motions and their velocity structures complicate the propagation of seismic waves, it is important for the prediction of strong ground motion and seismic hazard to determine the three-dimensional (3-D) velocity structures of these urban basins. This importance motivated various organizations to carry out extensive geophysical experiments and geological investigations, and velocity structure models are being constructed all over Japan. However, a study of a single dataset cannot completely define a 3-D velocity structure, so that we propose a standard procedure for modeling the 3-D velocity structure of an urban basin in Japan, by simultaneously and sequentially using various kinds of datasets such as those from refraction/reflection experiments, gravity surveys, surface geology, borehole logging, microtremor surveys, and earthquake records. We then apply the procedure to the Tokyo metropolitan area (TMA) over the Kanto basin with an area of about 17,000 km^2 and the maximum thickness of about 4 km. As one of the steps in the procedure, a joint inversion of refraction and gravity data has been formulated to determine the 3-D topography of interfaces of the sedimentary layers as well and lateral distribution of the basement slowness. We validate the constructed velocity structure model by comparison of observed and synthetic waveforms, since this modeling is carried out mainly for strong ground motion prediction. The proposed procedure including the joint inversion and validation with ground motion simulations works well for TMA, and the applicability of the standard procedure has been confirmed for regions with substantial data of experiments and earthquake records in Japan.

1. Introduction

Most metropolitan areas are located over large-scale sedimentary basins. For example, Tokyo, the capital city of Japan, and its metropolitan area are located in a large-scale sedimentary basin called the Kanto basin with an area of about 17,000 km^2 and the maximum thickness of about 4 km. The basement rocks are exposed in the Kanto, Tanzawa, Ashio and Yamizo mountains, which surround the basin on the west and north sides as shown in Fig. 1. It is mostly bounded by the Pacific ocean on the other sides as well, so the structure of the Kanto basin is three-dimensionally complicated. The basin and its surrounding areas are seismically active regions, where the Philippine Sea plate subducts under the continental plate and the Pacific plate underthrusts beneath the Philippine Sea plate. The damage in the Tokyo metropolitan area (TMA) itself from the 1923 Kanto earthquake, in Mexico City from the 1985 Michoacan earthquake, and in the Marina district of San Francisco from the 1989 Loma Prieta earthquake has clearly illustrated the risks for population centers located in basins (e.g., Olsen et al., 1995). The sediments filling the basins amplify ground motions and their structures complicate the propagation of seismic waves (e.g., Koketsu and Kikuchi, 2000), so it is important for the prediction of strong ground motion and seismic hazard to determine the three-dimensional (3-D) velocity structures of these urban basins.

This importance motivated extensive refraction experiments carried out in and around the Kanto basin from 1975 to 1988. Koketsu and Higashi (1992) compiled the traveltime data from the experiments and inverted them to recover the topography of the sediment/basement interface in the basin. Komazawa and Hasegawa (1988) compiled the results of gravity surveys, and recovered this topography using Bouguer anomalies. Suzuki (1996, 1999) collected geological sections and velocity logging data at deep boreholes for constructing a 3-D velocity structure model. Yamanaka and Yamada (2002) compiled the results of microtremor surveys including their own observations for determining the 3-D velocity structure of the shallow sediments. They also constructed the velocity model for the southernmost part of Fig. 1 using the results of Nishizawa et al. (1996). These investigations

* Corresponding author.
E-mail address: koketsu@eri.u-tokyo.ac.jp (K. Koketsu).
[1] Afnimar has only a single name according to the custom in Kalimantan, Indonesia.

0040-1951/$ – see front matter © 2008 Elsevier B.V. All rights reserved.
doi:10.1016/j.tecto.2008.05.037

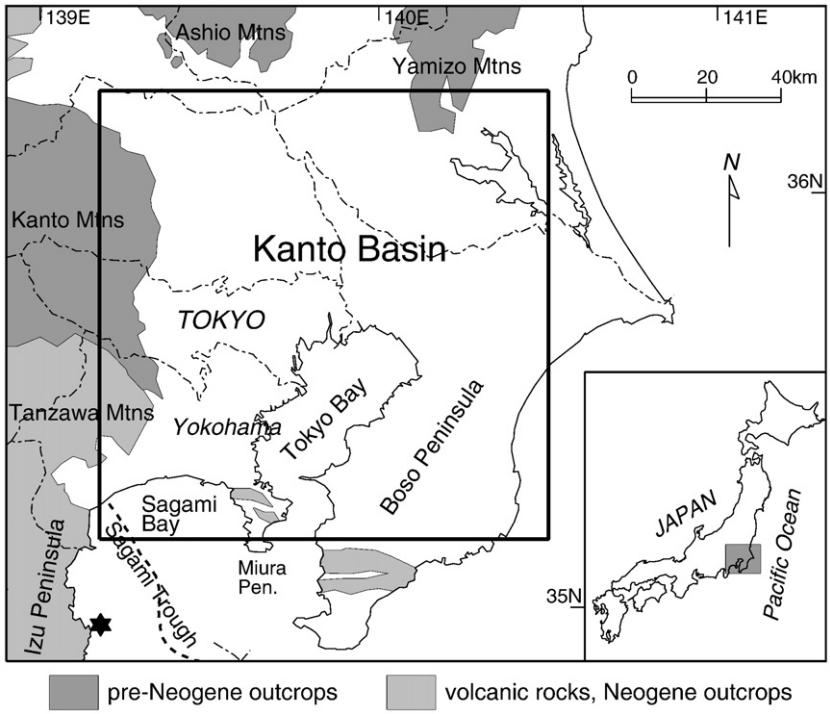

Fig. 1. Index map of the Kanto basin. The Pre-Neogene basement (dark), and the Neogene basement or volcanic rocks (light) outcrop in the grey zones, outlining the Kanto basin (Sugiyama et al., 1997). The rectangle drawn by thick lines is the 120×120 km target area of this study. The hexagram denotes the epicenter of the east off Izu peninsula earthquake in 1998.

are summarized that suggest three sedimentary layers in the Kanto basin and the total thickness of the sediments to be larger than 2 km in the region from the center to the northwestern part of the basin.

However, these studies cannot completely define the 3-D velocity structure. Koketsu and Higashi (1992), for example, noted that some model regions suffer ray coverage problem due to the irregular distribution of refraction data. We can overcome this problem by introducing the denser gravity data and jointly inverting them with the refraction data. Refraction data have the ability to resolve velocity structures in detail (e.g., Hole et al., 1992; Zelt and Borton, 1998) and precisely estimate seismic velocities and layer geometry (e.g., Zelt and Smith, 1992), but seismic surveys are too expensive to cover the whole area of a sedimentary basin. On the other hand, gravity surveys can be carried out more densely and homogeneously because of their portability, but they cannot measure seismic velocity directly, and the inversion of gravity data holds the inherent non-uniqueness of any geophysical method based upon a static potential field (e.g., Vigneresse, 1977). Afnimar et al. (2002) have developed a joint inversion scheme of refraction and gravity data for the 3-D shape of a sediment/basement interface assuming a relation between densities and seismic velocities. They showed that the joint inversion produces a better result than single-dataset inversions in its application to the Osaka basin, southwestern Japan. Parsons et al. (2001) developed a sequential inversion scheme of seismic traveltime and gravity data for a 3-D velocity structure, and applied it to the Seattle basin of Washington state, USA.

Therefore, we have to simultaneously or sequentially use various kinds of datasets for modeling the 3-D velocity structure of an urban basin. It is also necessary to verify a resultant model by seismic waveform studies, since this modeling is carried out mainly for strong ground motion prediction (e.g., Sato et al., 1999; Magistrale et al., 2000). We can calibrate velocity structure models by comparison of observed and synthetic dominant periods of spectral ratios and time history waveforms (e.g., Suzuki et al., 2005). Based on these experiences, we propose a standard modeling procedure in Japan, because extensive geophysical experiments and geological investigations have been carried out and velocity structure models are being constructed all over Japan. We then apply it to TMA for constructing a reference 3-D velocity structure model.

2. Modeling procedure

In seismology, two kinds of basement (bedrock) are defined in a velocity structure model. 'Seismic basement (bedrock)' is usually assigned to the uppermost part of the crust, whose S-wave velocity (V_S) is around 3 km/s, while 'engineering bedrock' with a V_S of 400 to 700 m/s is located just below surface layers. Regions between seismic basement and engineering bedrock are greatly influence long-period ground motion, so our modeling procedure targets these parts of subsurface velocity structures. Models for the crustal velocity structures from the seismic basement to the Moho discontinuity and the velocity structures of subducting plates must also be included to simulate strong ground motions from subduction-zone earthquakes.

If there are various kinds of exploration datasets and observed seismograms in such basins as the Kanto basin, we propose the following standard procedure used for their velocity structures in common. The applicability of this standard procedure for TMA will be examined in the next sections.

Step 1: Assume an initial layered model consisting of seismic basement and sedimentary layers from comprehensive overview of geological information, borehole data, and exploration results.

Step 2: Assign P-wave velocities to the basement and layers based on the results of refraction and reflection surveys, and borehole logging. Assign S-wave velocities based on the results of borehole logging, microtremor surveys, spectral-ratio analyses of seismograms, and empirical relationships between P- and S-wave velocities.

Step 3: Obtain the velocity structure right under engineering bedrock from the results of microtremor surveys referring to the results of borehole logging, since among 2-D or 3-D surveys only microtremor surveys are sensitive to shallow velocity distributions and the shapes of shallow interfaces.

Step 4: Compile data and information on faults and folds. Convert time sections from seismic reflection surveys and borehole logging into depth sections using the P- and S-wave velocities in Step 2.

Step 5: Determine the shapes of interfaces between the layers and basement by inversions of geophysical-survey data (e.g., refraction traveltimes and gravity anomalies). In case of insufficient data, forward modeling is carried out. The depths of faults and folds in Step 4 are introduced into the inversions as constraints, or additional data to the forward modeling.

Step 6: Calibrate the P-and S-wave velocities in Step 2 and the interface shapes in Step 5 by inversion or forward modeling of spectral features of observed seismograms such as dominant periods of H/V (horizontal/vertical) spectral ratios.

Step 7: Adjust the velocities and interface shapes using inversion or forward modeling of time history waveforms of observed seismograms.

Although sufficient exploration data may not be available except for major metropolitan areas, sufficient observed seismograms are always available for all the important sedimentary basins in Japan, thanks to the K-NET and KiK-net arrays (e.g., Kinoshita, 1998). In this case, stronger emphasis should be placed on Steps 6 to 7 than on Steps 3 to 5. The density of K-NET and KiK-net is high enough for the waveform modeling in Steps 6 and 7, but insufficiently low for traveltime tomography. Therefore, we do not use traveltimes from local earthquakes instead of traveltimes from refraction experiments, though we can incorporate them into the above joint inversion as supplementary data.

3. Initial velocity model (Steps 1 to 3)

At the first step of the application of the standard modeling procedure to TMA, we refer to Suzuki (1996), who suggested from geological surveys and borehole measurements that the sediments filling the Kanto basin can be divided into the Shimosa group (middle to late Pleistocene), Kazusa group (Pliocene to early Pleistocene) and Miura group (Miocene). We take this 3-layer structure overlaid by the basement (Paleogene or earlier) as an initial velocity model. We then introduce a grid with knot points distributed at (x_i, y_j) $(i=1,N_i; j=1,N_j)$ as shown in Fig. 2 and represent interfaces separating adjacent sedimentary layers or the sediments and basement with the 2-D Lagrange interpolation

$$H_k(x,y)=\sum_{p=i}^{i+1}\sum_{q=j}^{j+1} z_{p,q,k}\left(1-\left|\frac{x-x_p}{x_{i+1}-x_i}\right|\right)\left(1-\left|\frac{y-y_q}{y_{j+1}-y_j}\right|\right) \quad (1)$$

when (x, y) is located in a cell defined by x_i, y_j, x_{i+1}, and y_{j+1}. In the depth function $H_k(x, y)$ for the k-th interface $(k=1,N_k)$, $z_{p,q,k}$ stands for the interface depth at the knot (x_p, y_q). We distribute the knot points at an interval of 5 km. The interface shapes proposed by Suzuki (1999) are adopted as the initial guesses at Step 1 of the modeling procedure.

The optimal parameterization might be that all the interfaces, layer velocities and basement velocity are variable, but we cannot avoid trade-offs between the shapes of these interfaces and velocities in the sediments due to the limitation of the datasets. Accordingly, the P-wave velocities of the sediments are fixed to be 1.8 km/s, 2.4 km/s, and 3.2 km/s in the Shimosa, Kazusa, and Miura layers, respectively, based on the estimates of Suzuki (1996) from borehole measurements. For the basement, many authors (Yajima, 1981; Koketsu and Higashi, 1992; Suzuki, 1996; Yamanaka and Yamada, 2002) have found variable velocities, so we cannot model it with a fixed velocity. The basement slowness (inverse of P-wave velocity) at a point of (x, y) is defined by the 2-D Lagrange interpolation

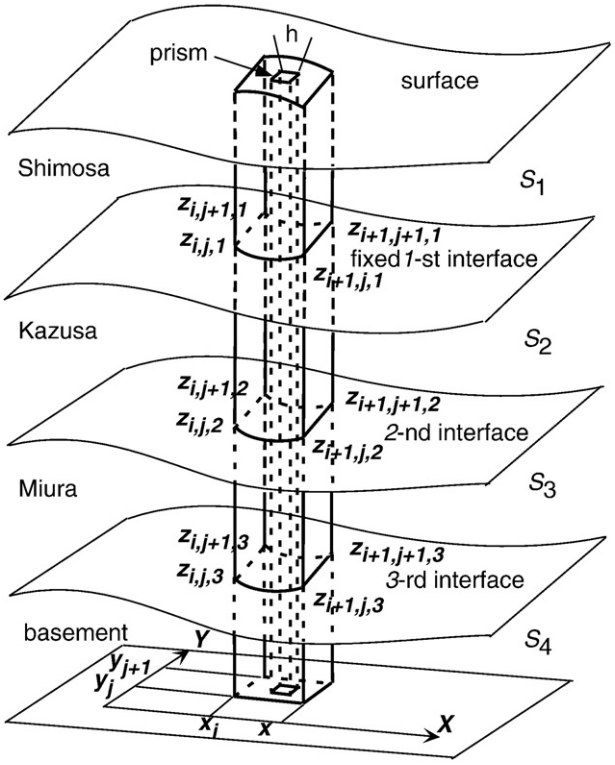

Fig. 2. Definition of the interface knots $(x_i, y_j, z_{i,j,k})$ for the k-th interface with the fixed sediment slownesses S_1 to S_3 and variable basement slowness S_4, and the rectangular prism with a cross section of $h \times h$ for gravity calculation.

$$S_4(x,y)=\sum_{p=I}^{I+1}\sum_{q=J}^{J+1} s_{p,q}\left(1-\left|\frac{x-x_p}{x_{I+1}-x_I}\right|\right)\left(1-\left|\frac{y-y_q}{y_{J+1}-y_J}\right|\right) \quad (2)$$

where $s_{p,q}$ stands for the slowness at the knot (x_p, y_q). We here distribute knot points for the basement rocks at an interval of about 20 km. Geological surveys suggest that the basement rocks are gradually younger toward the south because of tectonic accretion of the oceanic crust on the Philippine Sea plate to the continental plate (Fig. 3). Accordingly, we allow the basement velocity to vary in the model. We initially set it to be 5.7 km/s in the areas A, B and C of Fig. 3. 4.8 km/s is used in the areas D and E at Step 2 of the modeling procedure.

Finally, the S-wave velocities are fixed to be 0.4–0.6 km/s in the Shimosa layer, 1.0 km/s in the Kazusa layer, 1.7 km/s in the Miura layer based on the microtremor exploration by Yamanaka and Yamada (2002). Those in the Shimosa layer are spatially variable, and the result of Yamanaka and Yamada (2002) is again used for their distribution. The S-wave velocities in the basement are calculated by a linear relationship between P- and S-wave velocities ($V_S=0.93\ V_P-1.97$) that we obtained. These S-wave velocities and the P-wave velocities previously defined are in good agreement with Brocher's (2005) regression fit. The densities of the sedimentary layers, which are required for a joint inversion at Step 5, are also fixed to be 1.85 g/cm^3,

2.08 g/cm^3, and 2.28 g/cm^3 based on the borehole measurements compiled by Suzuki (1996, 1999) and the equation

$$\rho = a \ln S + b \tag{3}$$

of Nafe and Drake (1963) with $a = -0.536$ and $b = 1.635$ derived from their experimental data for sediments and sedimentary rocks.

At Step 3, the first interface separating the Shimosa and Kazusa layers is then fixed to the model constructed by Yamanaka and Yamada (2002) from microtremor observations (Fig. 6).

4. Data and constraints (Step 4)

Koketsu and Higashi (1992) used 1758 traveltimes of refraction arrivals from 62 shots. After the last shot of this series of refraction experiments in 1988, 27 new shots were fired additionally. The refraction dataset of this study consists of 7142 traveltimes from these 89 shots (Fig. 4a). Most of the traveltimes were picked with accuracy of 10 ms. Several authors (e.g., Yamanaka et al., 1988) found P-wave velocities as high as 6 km/s in the southern part of the lower basement. We exclude traveltimes accompanied by such high velocities, because they may correspond to arrivals traveling in deeper parts of the crust. We then carry out some test inversions of refraction data only, and traveltimes associated with residuals larger than 0.3 s are also excluded, since most of residuals in the result of Koketsu and Higashi (1992) are smaller than 0.3 s. Example record sections with traveltime curves are shown in Fig. 3 of Koketsu and Higashi (1992).

Komazawa and Hasegawa (1988) compiled dense gravity observations in and around the Kanto basin, and converted the observed data to absolute gravities based on the Japan Gravity Standard Network 1975. Fig. 4b shows a contour representation of free-air anomalies, which they derived from these gravity data and the Tokyo Datum 1967. We pick 456 anomalies at nearly constant intervals as shown in this figure.

To reduce the ambiguity in a solution of the joint inversion of refraction and gravity data at Step 5, it is essential to introduce interpretations of geological or geophysical data other than refraction traveltimes and gravity anomalies. Suzuki (1996, 1999) compiled the interpretations of borehole observations. Nishizawa et al. (1996) conducted seismic refraction surveys in the Sagami bay and provided us with their interpretations. The structures at the points of these observations are constrained to be close to the interpretations. Sugiyama et al. (1997) compiled results of geological surveys in and around the Kanto basin and specified outcrops of Pre-Neogene or Neogene basement and volcanic rocks in the grey zones of Fig. 1. We distribute points in the zones and the basement depth is constrained to be the height of the surface at these points, except for the Miura peninsula, where no high gravity anomaly is observed (Fig. 4b). Fig. 5 summarizes the constraints for the inversion.

5. Method of joint inversion (Step 5-1)

Equations relating a density ρ with a P-wave slowness S are required for a joint inversion of seismic and gravity data at Step 5 of the modeling procedure. We adopt the linear equation of Tondi et al. (2000) for P-wave velocities of 4.8 to 5.7 km/s, because only the velocities in the basement are variable in our formulation. We then convert this equation into the linear relationship between density and slowness

$$\rho = c\, S_4 + d \tag{4}$$

in order to reduce nonlinearity of the inversion. The coefficients of Eq. (4) will be determined by a joint inversion with the initial values of $c = -7.233$ and $d = 3.869$.

In order to calculate refraction traveltimes, we use the finite difference scheme of Vidale (1990) with the revisions by Hole and Zelt (1995), Podvin and Lecomte (1991) and Afnimar and Koketsu (2000). The spacing of the finite difference grid is 0.1 km, which is much finer than the knot interval of the model parameterizations in Eqs. (1) and (2). Rays are traced through wavefronts by using the backward-tracing method developed by Afnimar et al. (2002). Similarly to the derivatives

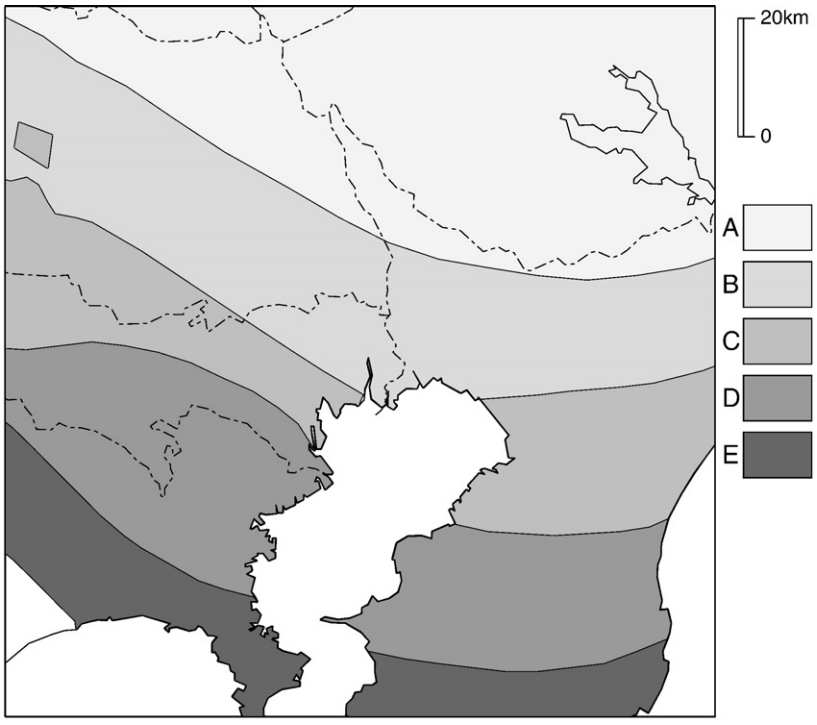

Fig. 3. A geological interpretation of the structure in the basement (Yajima, 1981). The parts shaded with five different tones correspond to (A) Ryoke metamorphic belt, (B) Sanbagawa metamorphic belt, (C) Chichibu belt, (D) northern Shimanto belt and (E) southern Shimanto belt, respectively. We initially set the P-wave velocity to be 5.7 km/s at the basement in the areas A, B and C, and 4.8 km/s in the areas D and E.

at a sediment/basement interface in Afnimar et al. (2002), the derivatives of a traveltime t with respect to $z_{i,j,k}$ can be written as

$$\frac{\partial t}{\partial z_{i,j,k}} = \frac{\partial t}{\partial d}\frac{\partial d}{\partial H_k}\frac{\partial H_k}{\partial z_{i,j,k}}$$
$$\frac{\partial t}{\partial d} = S_k \cos\theta_1 - S_{k+1}\cos\theta_2, \quad \frac{\partial d}{\partial H_k} = \cos\varphi \tag{5}$$
$$\frac{\partial H_k}{\partial z_{i,j,k}} = \left(1 - \left|\frac{x^c - x_i}{x_{i+1} - x_i}\right|\right)\left(1 - \left|\frac{y^c - y_j}{y_{j+1} - y_j}\right|\right),$$

where d is a small movement of the interface at a ray crossing (ray-interface intersection) along the direction normal to the interface. As in Eq. (1), H_k and $z_{i,j,k}$ stand for the depths of the ray crossing on k-th interface and the knot point at (x_i, y_j), respectively. φ is the angle between the interface and horizontal plane at the ray crossing. θ_1 and θ_2 denote the angles of incidence and refraction, respectively.

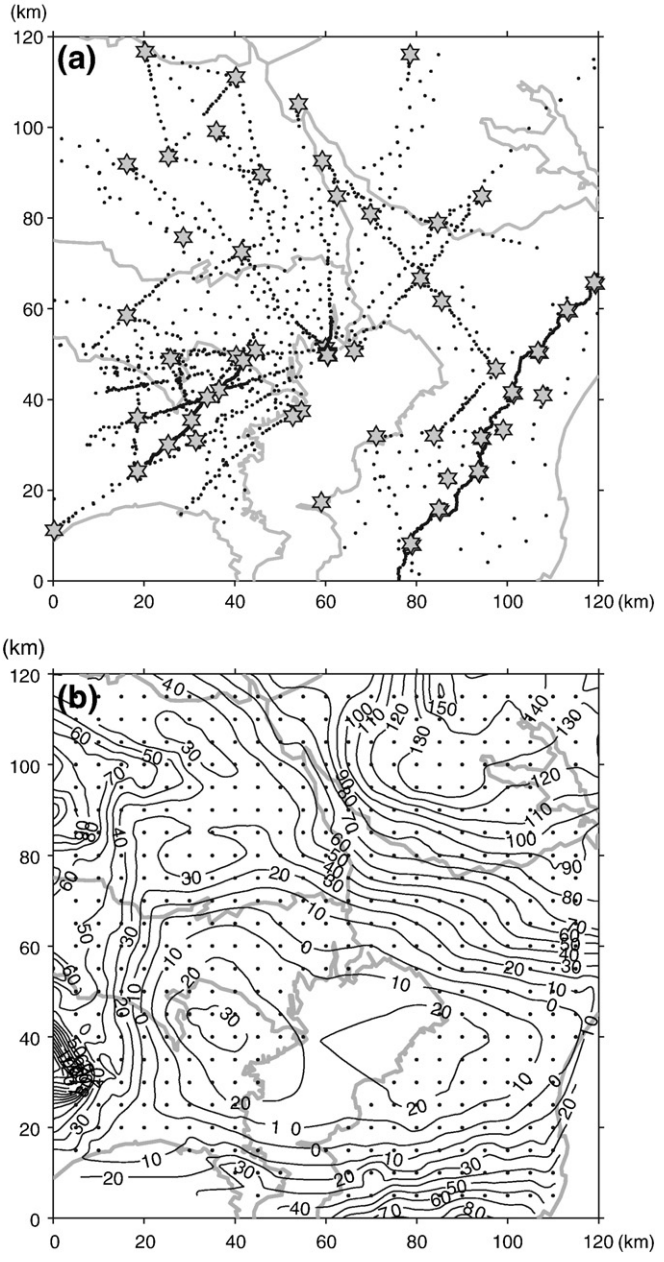

Fig. 4. (a) Distribution of the shots (hexagrams) and receivers (small dots) of the refraction experiments in the Kanto area. (b) Observed free-air gravity anomalies in mgal (contours) and data points for the joint inversion (small dots).

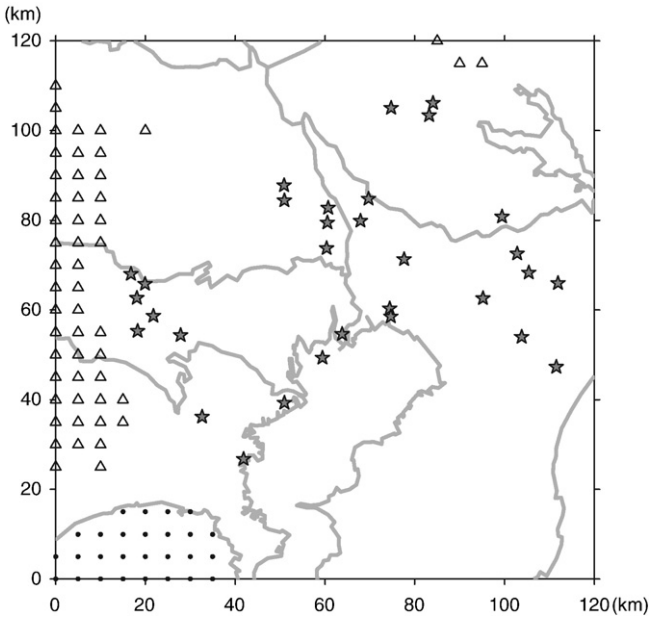

Fig. 5. Points of the constraints for the inversion. The structures at the star symbols and small dots are constrained to be close to the interpretations of borehole, reflection and refraction surveys. The basement depths are constrained to be the heights of the surface at the triangles.

This geometry is schematically illustrated in Fig. A1 of Zelt and Smith (1992). S_k and S_{k+1} are the slownesses of upper and lower layers at the ray-interface intersection. x^c and y^c represent the x-and y-coordinates of the ray crossing.

In this study, the derivatives with respect to the basement slownesses $s_{I,J}$ are required. We introduce no vertical velocity gradient into the basement, so that all refraction arrivals from the basement are head waves and the derivatives can be written as

$$\frac{\partial t}{\partial s_{I,J}} = \frac{\partial t}{\partial S_4}\frac{\partial S_4}{\partial s_{I,J}}, \tag{6}$$

where $\partial t/\partial S_4$ is the length of a ray in a cell of the basement surrounded by the four knots at (x_I, y_J), (x_{I+1}, y_J), (x_I, y_{J+1}) and (x_{I+1}, y_{J+1}). An approximate of $\partial S_4/\partial s_{I,J}$ is given from Eq. (2) as

$$\frac{\partial S_4}{\partial s_{I,J}} = \left(1 - \left|\frac{x^m - x_I}{x_{I+1} - x_I}\right|\right)\left(1 - \left|\frac{y^m - y_J}{y_{J+1} - y_J}\right|\right), \tag{7}$$

where x^m and y^m are the x-and y-coordinates of the middle point of the ray.

For gravity anomalies, the target region is partitioned into many rectangular prisms with cross sections of $h \times h$ as shown in Fig. 2. A prism extends from the surface to the basement, being divided into three parts by the sedimentary layers. The k-th part of the p-th prism generates the gravity anomaly

$$g_{p,k} = G\Delta\rho_{p,k}\, g^{\mathrm{unit}}_{p,k} \tag{8}$$

where G is Newton's gravitational constant and $\Delta\rho_{p,k}$ is the relative density of the k-th part to the average basement density. $g^{\mathrm{unit}}_{p,k}$ is a non-linear function with respect to the geometry of the k-th part as described by Talwani (1973). The total gravity anomaly g is then the sum of anomalies from the parts of all the prisms:

$$g = G\sum_{p=1}^{P}\sum_{k=1}^{3}\Delta\rho_{p,k}\, g^{\mathrm{unit}}_{p,k} \tag{9}$$

where P is the total number of prisms.

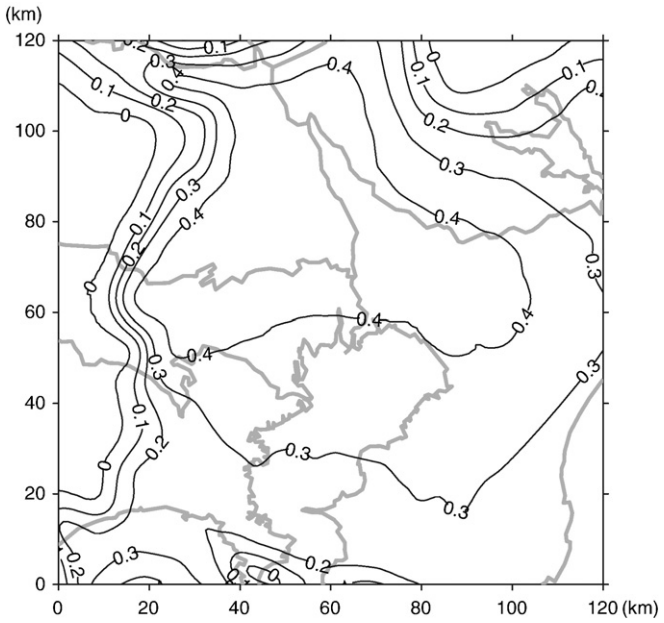

Fig. 6. Contours representation of the depth (in km) of the fixed first (Shimosa/Kazusa) interface determined by Yamanaka and Yamada (2002).

The derivative of a gravity anomaly g with respect to the k-th interface depth at the (i, j) knot point is defined by the chain derivative

$$\frac{\partial g}{\partial z_{i,j,k}} = \frac{\partial g}{\partial H_k}\frac{\partial H_k}{\partial z_{i,j,k}}. \tag{10}$$

$\partial H_k/\partial z_{i,j,k}$ is identical to that in Eq. (5) and $\partial g/\partial H_k$ was given by Talwani (1973). The derivative with respect to the slowness at the (I, J) knot point can be calculated from

$$\frac{\partial g}{\partial s_{I,J}} = \sum_{p\in(I,J)} \frac{\partial g}{\partial \Delta\rho_{p,4}}\frac{\partial \Delta\rho_{p,4}}{\partial S_4}\frac{\partial S_4}{\partial s_{I,J}}. \tag{11}$$

Using Eqs. (4) and (9) we obtain

$$\frac{\partial g}{\partial \Delta\rho_{p,4}}\frac{\partial \Delta\rho_{p,4}}{\partial S_4} = Gc\, g^{\mathrm{unit}}_{p,4} \tag{12}$$

for the basement part of the p-th prism. $\partial S_4/\partial s_{I,J}$ is identical to that in Eq. (7). The derivative with respect to the coefficients in Eq. (4) is defined as

$$\frac{\partial g}{\partial c} = \frac{\partial g}{\partial \Delta\rho_{p,4}}\frac{\partial \Delta\rho_{p,4}}{\partial c} = GS_4\, g^{\mathrm{unit}}_{p,4} \tag{13}$$

$$\frac{\partial g}{\partial d} = \frac{\partial g}{\partial \Delta\rho_{p,4}}\frac{\partial \Delta\rho_{p,4}}{\partial d} = G\, g^{\mathrm{unit}}_{p,4} \tag{14}$$

using Eqs. (4) and (9).

The depths of the interface knots and the slownesses at the basement knots will be determined simultaneously by a joint inversion. We first linearize the observation equations of this inversion as

$$\begin{aligned}
&\sum_i\sum_j\sum_k \frac{\partial t_m}{\partial z_{i,j,k}}\Delta z_{i,j,k} + \sum_I\sum_J \frac{\partial t_m}{\partial s_{I,J}}\Delta s_{I,J} \sim \Delta t_m \\
&\sum_i\sum_j\sum_k \frac{\partial g_n}{\partial z_{i,j,k}}\Delta z_{i,j,k} + \sum_I\sum_J \frac{\partial g_n}{\partial s_{I,J}}\Delta s_{I,J} \\
&\qquad + \frac{\partial g_n}{\partial c}\Delta c + \frac{\partial g_n}{\partial d}\Delta d \sim \Delta g_n
\end{aligned} \tag{15}$$

using the depth corrections $\Delta z_{i,j,k}$, slowness corrections $\Delta s_{I,J}$, coefficient corrections Δc and Δd, traveltime residuals Δt_m and gravity

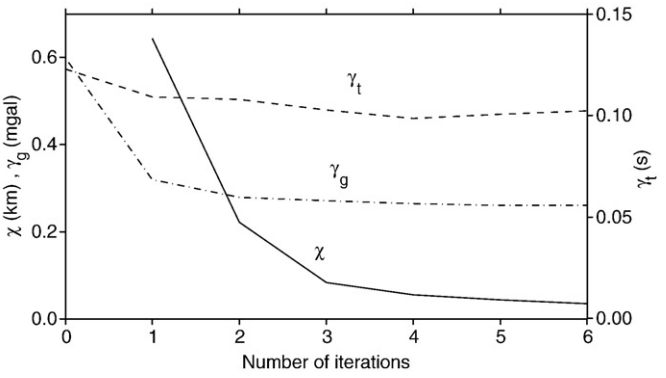

Fig. 7. The progress of RMS difference between the current and previous depth solutions χ (solid line), RMS traveltime residual γ_t (dashed line) and RMS gravity residual γ_g (dash-dotted line) during the iterations of the joint inversion.

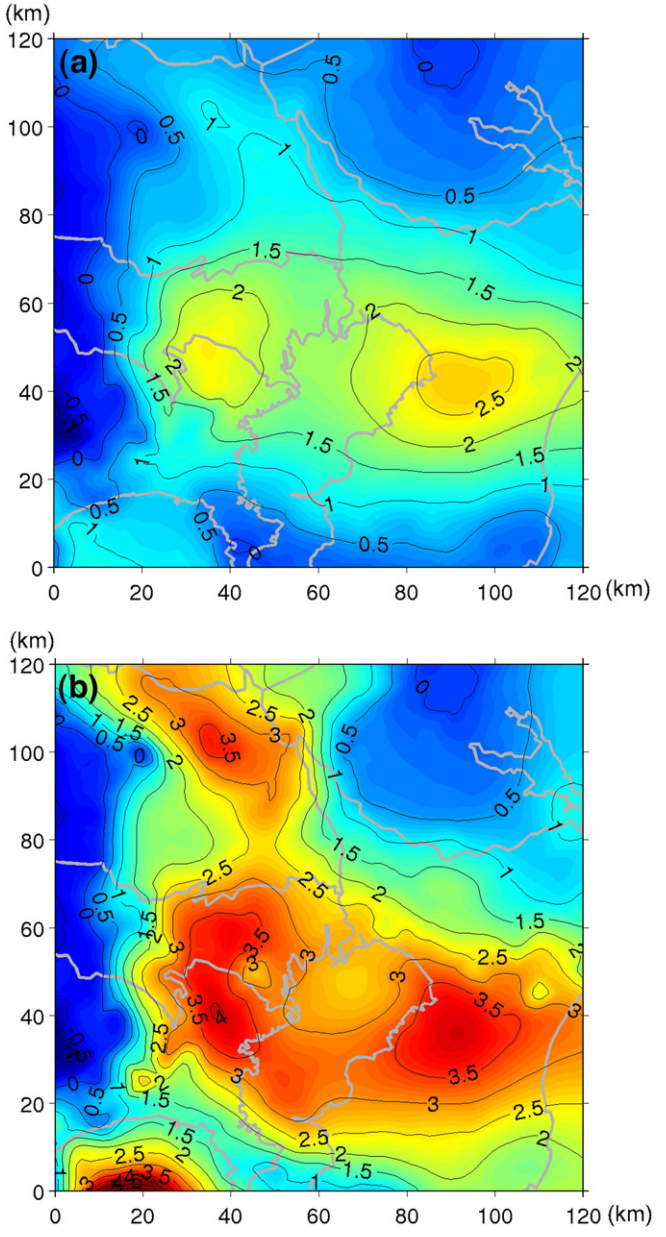

Fig. 8. Resultant depth distributions (in km) of (a) the second (Kazusa/Miura) interface and (b) the third (Miura/basement) interface.

residuals Δg_n. We then impose the following constraints on the inversion to avoid oscillatory artifacts in a solution and minimize non-uniqueness. We regularize the interface shapes and the basement slowness distribution by adding the linear equations

$$\begin{aligned} &z_{i,j,k} \sim z_{i+1,j,k}, \quad z_{i,j,k} \sim z_{i,j+1,k} \\ &s_{I,J} \sim s_{I+1,J}, \quad s_{I,J} \sim s_{I,J+1}. \end{aligned} \tag{16}$$

In order to recover a similar pattern to that of Fig. 2 in the distribution of the basement slowness, we keep the slowness gradients standing by applying the second-order constraints

$$\begin{aligned} &s_{I-1,J} - 2\,s_{I,J} + s_{I+1,J} \sim 0, \\ &s_{I,J-1} - 2\,s_{I,J} + s_{I,J+1} \sim 0. \end{aligned} \tag{17}$$

Secondly, the interface depths at the points indicated in Fig. 5 are constrained to be those derived from a priori information as

$$z_{i,j,k} \sim D_{i,j,k}. \tag{18}$$

We collectively represent $\Delta z_{i,j,k}$, $\Delta s_{I,J}$ with Δc and Δd, Δt_m and Δg_n by Δz, Δs, Δt and Δg, respectively. The joint inversion is now formulated by

$$\begin{pmatrix} \mathbf{A}_t \\ \mu_0 \mathbf{A}_g \\ \mu_1 \mathbf{A}_1 \\ \mu_2 \mathbf{A}_2 \\ \mu_3 \mathbf{A}_3 \end{pmatrix} \begin{pmatrix} \Delta z \\ \Delta s \end{pmatrix} \sim \begin{pmatrix} \Delta t \\ \mu_0 \Delta g \\ \mu_1 b_1 \\ \mu_2 b_2 \\ \mu_3 b_3 \end{pmatrix} \tag{19}$$

where μ_0, μ_1, μ_2 and μ_3 are respectively the relative weights of the gravity observation equation, the linear, second-order and absolute constraints to the traveltime observation equation. The matrix $\mathbf{A}_t$ or $\mathbf{A}_g$ consists of the derivatives in Eqs. (5) and (6), or Eqs. (10), (11), (13) and (14). The elements of $\mathbf{A}_1$, $\mathbf{A}_2$ and $\mathbf{A}_3$ are the derivatives of Eqs. (16), (17), and (18) with respect to $z_{i,j,k}$ or $s_{I,J}$. We solve the matrix equation (19) in a least-squares sense using the code called LSQR (Paige and Saunders, 1982). Since the problem is non-linear, this matrix inversion is iteratively repeated until convergence.

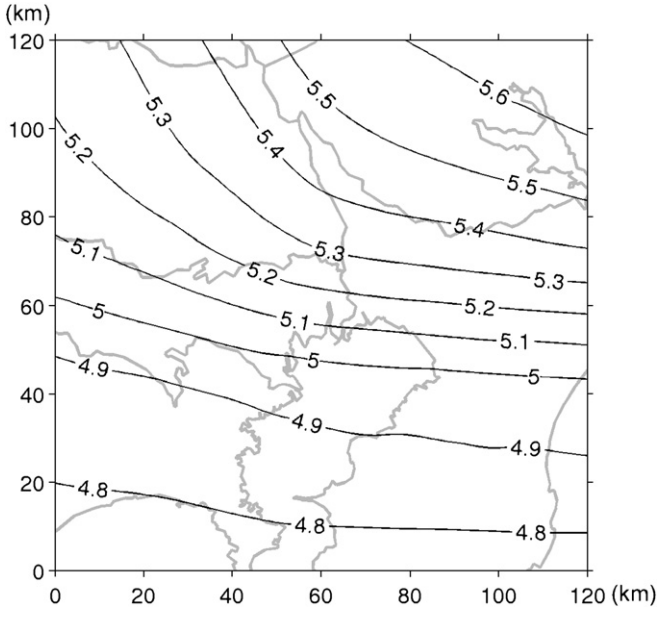

Fig. 9. Distribution of the resultant P-wave velocity (in km/s) in the basement.

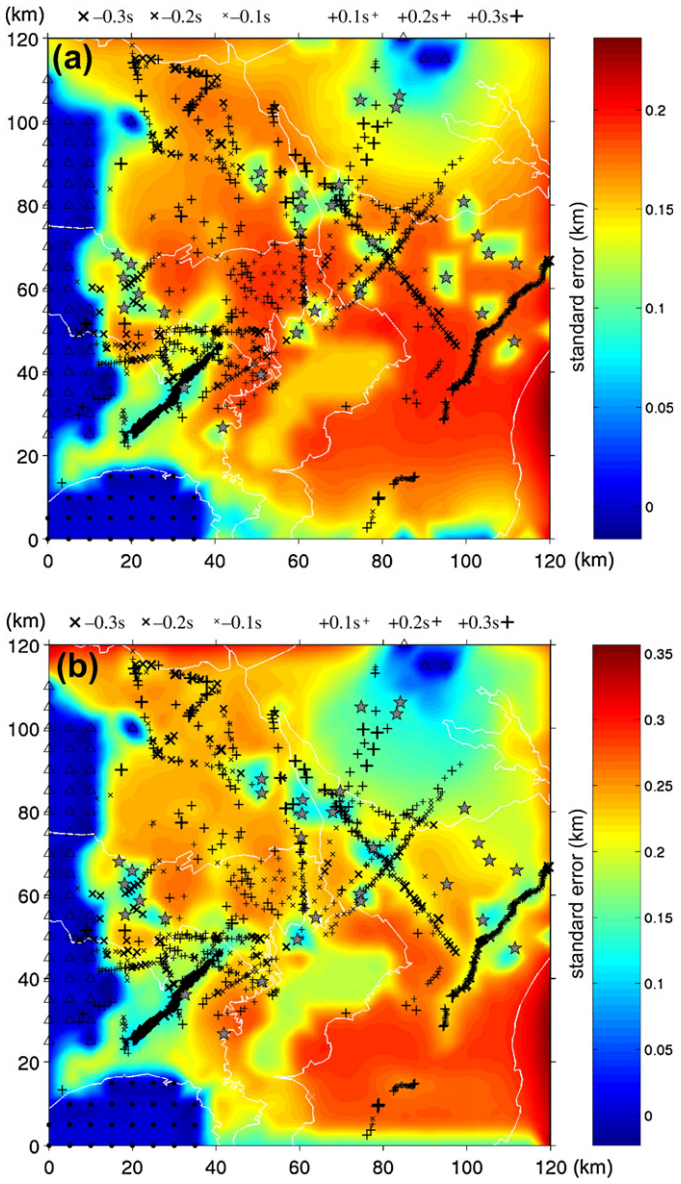

Fig. 10. Standard error of resultant depth of (a) the second (Kazusa/Miura) interface and (b) the third (Miura/basement) interface. Crosses and plus signs indicate negative and positive traveltime residuals, respectively. Star symbols and small dots represent the points of the constraints for the inversion as in Fig. 5.

We calculate the RMS (root mean square) difference of the current and previous interface depths

$$\chi = \sqrt{\frac{1}{N_i N_j N_k} |\Delta z|^2}, \tag{20}$$

and the RMS traveltime and gravity residuals

$$\gamma_t = \sqrt{\frac{1}{N_t} |\Delta t|^2}, \quad \gamma_g = \sqrt{\frac{1}{N_g} |\Delta g|^2} \tag{21}$$

at each iteration. If no further improvement is expected for them, the computation will be terminated. The standard error of the final solution can be estimated by taking the square roots of the diagonal elements of the covariance matrix

$$\mathbf{C} = \sigma_t^2 \left(\mathbf{A}_t^{\mathrm{T}} \mathbf{A}_t + \mu_0^2 \mathbf{A}_g^{\mathrm{T}} \mathbf{A}_g + \mu_1^2 \mathbf{A}_1^{\mathrm{T}} \mathbf{A}_1 + \mu_2^2 \mathbf{A}_2^{\mathrm{T}} \mathbf{A}_2 + \mu_3^2 \mathbf{A}_3^{\mathrm{T}} \mathbf{A}_3 \right)^{-1}. \tag{22}$$

The traveltime variance σ_t^2 in the above is estimated from

$$\sigma_t^2 = \left[|\Delta t|^2 + \mu_0^2(\Delta g)^2 + \mu_1^2 b_1^2 + \mu_2^2 b_2^2 + \mu_3^2 b_3^2\right] / \left(N_t + N_g + N_1 + N_2 + N_3 - M\right), \quad (23)$$

where M is the number of model parameters (Yoshida and Koketsu, 1990; Afnimar et al., 2002).

6. Results of joint inversion (Step 5-2)

We carried out joint inversions for twenty sets of weights, and chose the best inversion by comparing Akaike's (1980) Bayesian Information Criteria (see Koketsu and Higashi (1992) for details of ABIC). We performed six iterations for this optimum joint inversion. Fig. 7 shows the RMS difference between the current and previous depth solutions χ, RMS traveltime residual γ_t and RMS gravity residual γ_g for each iteration. χ, γ_t and γ_g do not change significantly after the third iteration, so the inversion result from this iteration is chosen as the final solution at Step 5 of the modeling procedure. The resultant interface shapes and basement velocity distribution are shown in Figs. 8 and 9, respectively. The coefficients of the density-slowness relation in the basement were determined to be $c = -6.737$ and $d = 3.808$.

We estimate the standard errors of the final solutions using Eqs. (22), (23) and a matrix inversion code, and plot them in Figs. 10 and 11. Most of the small interface errors (blue zones in Fig. 10) are related to the absolute constraints shown with star symbols and small dots as in Fig. 5. The diagonal blue zones in the southwestern and southeastern parts are due to the dense distributions of small traveltime residuals from recent refraction experiments, which are plotted with crosses and plus signs. In the areas where sufficient refraction data are available, the standard error of the third (Miura/basement) interface depth is smaller than that for the second (Kazusa/Miura) interface. This implies that the refraction data work better in the deeper part. Many refraction rays traverse the basement, so that the basement velocity is well determined and the standard error of the basement velocity is as low as 0.01–0.02 km/s, in particular, around the center of the target region.

Thick sediments are imaged in the southern part around the Tokyo bay. Their thickness is determined to be about 3 km with a standard error of about 0.3 km. They extend to the north through the downtown of Tokyo, and turn to the west in the northernmost part. Compared to the results of the traveltime inversion (Koketsu and Higashi, 1992) and borehole measurements (Suzuki, 1996), the detailed topography of the interfaces is recovered in Fig. 8. The complicated pattern of the Miura/basement interface of our result around Yokohama in the southern part is consistent with a model from seismic waves PS-converted at this interface (Miura and Midorikawa, 2001).

We here note some differences between our model and these previous results. The Miura/basement interface in the southeastern part is shallower than the previous results, and its deepest point in this part is shifted to the north. On the other side, the interfaces in the southwestern and northwestern part are deeper than the previous results. These differences come from the modeling improvements in our joint inversion, that are the multilayer structure, variable basement velocity, introduction of the Shimosa layer and so on. The gravity data and new refraction data should also play important roles. Since there is only few refraction data in the northeastern part, the gravity data control the model in this part (Fig. 4).

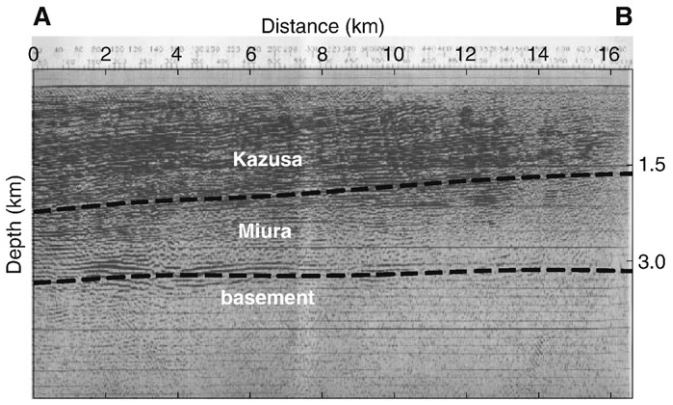

Fig. 12. Cross section of the obtained 3-D structure (dashed lines) and seismic reflection profile along the A–B lines in Fig. 13.

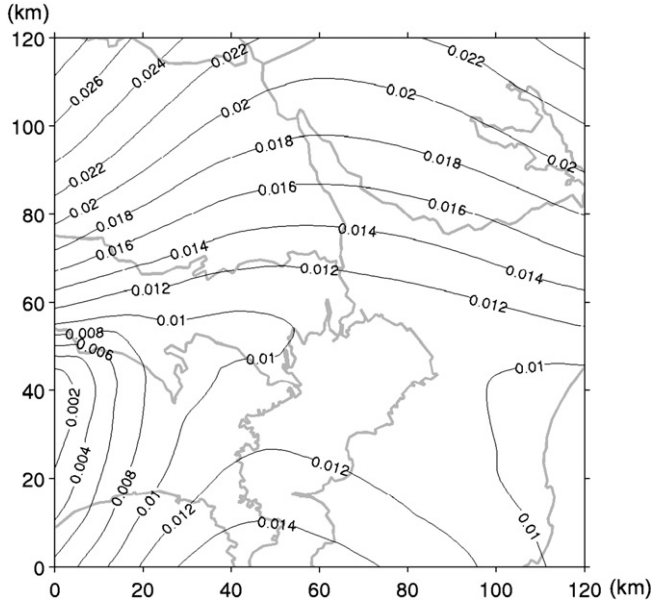

Fig. 11. Standard error of the P-wave velocity (km/s) in the basement.

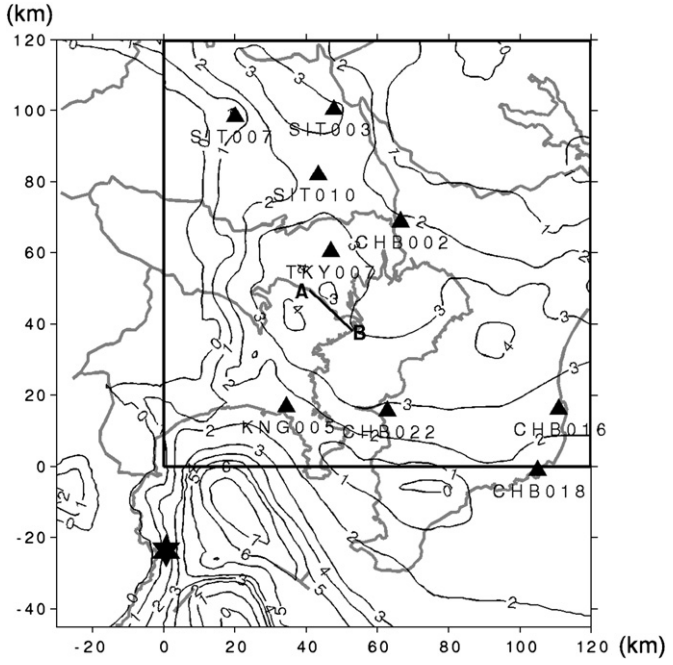

Fig. 13. Distribution of ground motion seismometers (triangle) that recorded the magnitude 5.7 earthquake on May 3, 1998 (hexagram). Black rectangle is our study area where the joint inversion is conducted. Another reflection survey was carried out along the A–B lines.

Yajima (1981) interpreted geological surveys as shown in Fig. 3. He divided the basement in the Kanto region into five belts, which are the southern Shimanto (Tertiary), northern Shimanto (Cretaceous), Chichibu (Jurassic), Sanbagawa metamorphic (Jurassic) and Ryoke metamorphic (Triassic) belts. Therefore, the age of basement rocks increases from Miocene of Tertiary in the southernmost part to Triassic in the northernmost part. This distribution is in good agreement with the recovered basement velocity, which increases from 4.8 km/s in the south to 5.7 km/s in the north (Fig. 9), if we assume that younger rocks have lower velocities. The basement of the central Japan is considered to be built up by the accretion of oceanic sediments from the subducting Philippine Sea plate (e.g., Taira et al., 1981). The above distributions of velocity and rock age also agree with this tectonic interpretation. The Izu peninsula on the Philippine Sea plate moves northward without subduction and collides with the continental plate. This collision deforms the east–west pattern of the five belts in the north of the peninsula. We can also find such deformation in the western part of the basement velocity distribution (Fig. 9).

Large-scale reflection experiments were conducted in TMA in the 1990s and later (e.g., Sato et al., 2005), but only a few of them were used in this study. Fig. 12 shows a depth profile from one of the unused survey results, which was carried along the A–B lines in Fig. 13. We make a cross section of the obtained 3-D structure and superimpose it directly onto the above profile for comparison. A clear reflection in the profile at a depth of 3 km obviously corresponds to the Miura/basement interface in the cross section. There is a strongly reflective zone in the shallow part of the profile and its lower boundary is located at depths of 2 and 1.5 km under points A and B, respectively. This boundary probably corresponds to the Kazusa/Miura interface in the cross section.

7. Ground motion simulation (Steps 6 to 7)

As Steps 6 and 7 of the modeling procedure, we here validate the obtained 3-D model for prediction of seismic ground motions. The best way for this is to simulate those of an actual earthquake with the 3-D model and compare the results with observed records. On May 3, 1998, a magnitude 5.9 earthquake occurred at a depth of 5 km east off the Izu peninsula (a solid hexagram in Fig. 1) with focal mechanism of strike: 165°, dip: 85°, and rake: 8°, and a seismic moment of 2.35×10^{17} N m as reported by the Japan Meteorological Agency and National Research Institute for Earth Science and Disaster Prevention (NIED). The ground motions from this earthquake were observed by more than three hundred strong motion seismometers (Koketsu and Kikuchi, 2000).

Since the earthquake is located out of the study area of our joint inversion as shown in Fig. 13, we adopt the model by Yamanaka and

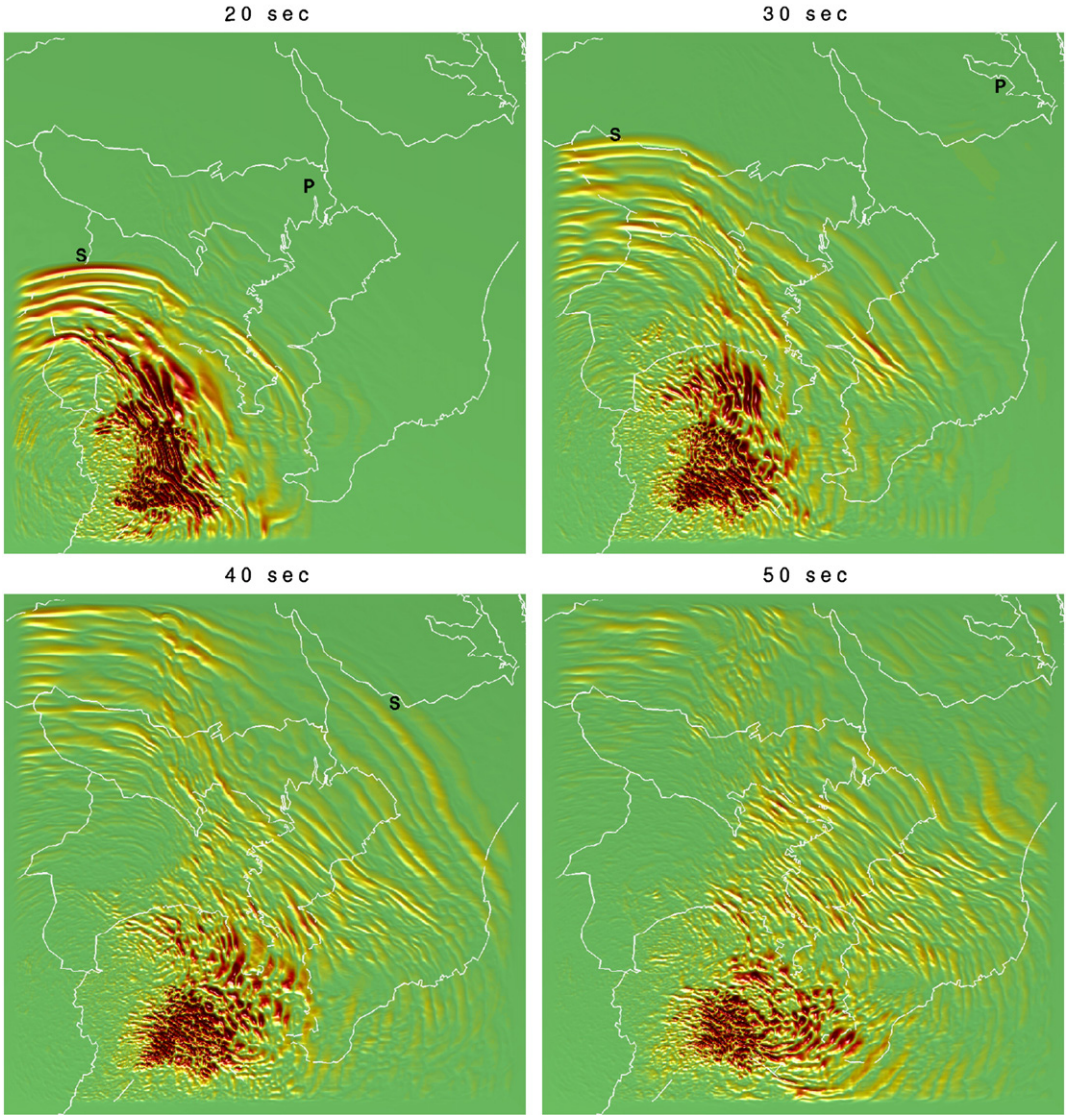

Fig. 14. Snapshots of the EW component of simulated ground velocity at 20, 30, 40 and 50 s after the earthquake, respectively. P and S indicate the wavefronts of P and S waves.

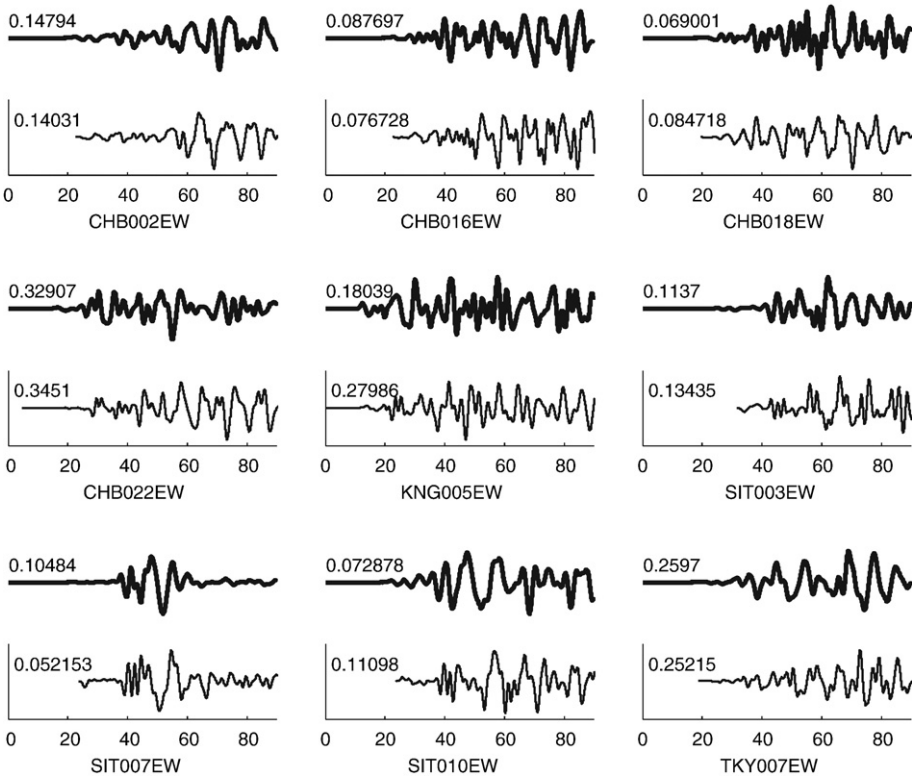

Fig. 15. Comparison of EW component of observed ground velocity (lower thin line) and simulated result (upper thick line). The number at the left side of each seismogram is the absolute maximum amplitude in cm/s.

Yamada (2002) for the western and southern margins. Its elastic properties are assumed to be the same as those derived by the joint inversion. We use the model by Sato et al. (1999) for the deeper crust. Topography is not included because of the rather flat surface of the Kanto basin, but we include intrinsic attenuation referring to Kohketsu and Shima (1985) and Sato et al. (1999). The simulation is conducted in a 153.6 by 153.6 by 38.4 km volume, which is discretized at an interval of 0.3 km. The lowest velocity in the volume is 0.6 km/s for S waves in the Shimosa layer, so that this interval is equivalent to four nodes per the minimum wavelength at a frequency of 0.5 Hz. The computation is carried out by a hybrid approach based on the PSM (pseudospectral method) formulation in horizontal coordinates and the conventional fourth-order FDM (finite difference method) scheme in depth (Furumura et al., 2002). If the volume is partitioned into subdomains along the depth axis, this hybrid PSM/FDM approach minimizes interprocessor communication overheads in parallel implementation and numerical dispersion in the horizontal coordinates.

We complete the 90 s (11,250 time steps) of simulated ground motion shown in Figs. 14 and 15. The faulting of the earthquake is a nearly vertical strike slip oriented north and south. Since this kind shallow earthquake generates well developed Love waves in the east–west (EW) direction, we plot snapshots and synthetic seismograms of the EW component of ground velocity. The snapshots in Fig. 14 show the developing complexity of ground motions as seismic waves propagate through the 3-D structure of the Kanto basin. At 20 s, the primary effect of the structure appears as delays in the arrivals of direct P and S waves around the center of the basin. This leads to the complex shapes of the wavefronts in the western margin of the Kanto basin. Some diffracted waves are generated at the western edge of the basin between the P and S wavefronts. The S wave is also followed by multiply reflected arrivals.

The surface wave trains, which mainly consist of Love waves, emerge into the Kanto basin from the Sagami bay at 30 s. They propagate through the basin at 40 s and 50 s, and their wavefronts are again distorted in the western margin due to the lateral heterogeneity of the structure from the western mountains to the basin center. Later portions of the surface wave trains propagate very slowly and they look almost standing in the region of the Sagami bay to Yokohama along the Miura peninsula and the western coast of the Tokyo bay. Koketsu and Kikuchi (2000) visualized the propagation of the Love wave using the observed ground motion records. The above features of the simulated surface waves agree with this visualization.

Thin lines in Fig. 15 represent the ground motions observed by strong motion seismometers at six stations of K-NET developed by NIED (Kinoshita, 1998). These stations are plotted with triangles in Fig. 13. All the acceleration records are converted to velocity seismograms and low-pass filtered with a cut-off frequency of 0.5 Hz. Except for CHB002 and KNG006, P-wave portions are missing, since the seismometers were triggered by the S-wave arrival and the delay time of 15 s is not sufficient to cover the P-wave portions. Our simulated results are plotted by thick lines in Fig. 15 and show fairly close agreement with observed seismograms, though we have not yet carried out inversions or forward modeling of spectral features and time history waveforms of observed seismograms but just the ground motion simulation at Steps 6 to 7. Since Love waves are dominant in the seismograms of Fig. 15, this agreement implies that our joint inversion and the microtremor exploration by Yamanaka and Yamada (2002) well recovered the actual S-wave velocity structure. In other words, the S-wave velocities of the shallow sedimentary layers are the most important for this agreement. However, in the portion of the direct S wave, its amplitude is somewhat overestimated. This discrepancy may come from problems in the modeling for the southernmost part of Fig. 1. We rely on the model of Yamanaka and Yamada (2002) for this region, but the model still requires further adjustments.

8. Discussion and conclusions

We proposed the standard procedure of velocity structure modeling in Japan, and applied it to TMA. At Steps 1 to 4 of this

procedure, we modeled the 3-D velocity structure in TMA assuming two variable interfaces, one fixed interface, fixed velocities in the sediments, and a laterally heterogeneous basement. The joint inversion of refraction and gravity data has been formulated for the 3-D topography of interfaces and lateral distribution of a basement slowness for Step 5 of the procedure. The resultant interfaces show more details of their shapes than previous models. The resultant basement velocity increases from the south to the north. This agrees with the geological setting in TMA, where the age of basement rocks increases from the south to the north.

At Steps 6 to 7, strong ground motion simulations were carried out for a magnitude 5.9 earthquake using the 3-D model by the joint inversion of Step 5. The snapshots of simulated ground motion recover most of the features in the observed ground motion propagation. The synthetic seismograms from the simulations also compare favorably with the observed seismograms, but the amplitudes of the direct S waves are somewhat overestimated.

Our joint inversion is preliminary, because our search for the minimum ABIC is rather limited and we could not perform resolution analyses or their alternatives such as checkerboard tests. We also have to further revise the velocity structure model for improving the agreement between the simulated and observed seismograms. We would leave these problems to more complete applications of the standard modeling procedure in the future.

The standard procedure proposed here is subject to the subsurface velocity structure modeling, but it is capable to be extended into crustal velocity structures if the quality and quantity of exploration datasets and observed seismograms are enough. An extension to reflection traveltimes is also straightforward.

Acknowledgments

We thank Shuhei Okubo for his kind suggestions and discussions on gravity anomalies. Masao Komazawa kindly provided us with the gravity data. Thoughtful comments by Tom Brocher, Michael Behm, and the guest editors greatly improved the manuscript. This research was supported by the Japan Science and Technology Corporation under the ACT-JST program 13C-2, the DaiDaiToku Project I of the MEXT, Japan, and the Integrated Velocity Structures Database Project sponsored by the Special Coordination Funds for Promoting Science and Technology.

References

Afnimar, Koketsu, K., 2000. Finite-difference traveltime calculation for head waves traveling along an irregular interface. Geophys. J. Int. 143, 729–734.

Afnimar, Koketsu, K., Nakagawa, K., 2002. Joint inversion of refraction and gravity data for the three-dimensional topography of a sediment-basement interface. Geophys. J. Int. 151, 243–254.

Akaike, H., 1980. Likelihood and Bayes procedure. In: Bernard, J.M., De Groot, M.H., Lindley, D.U., Smith, A.F.M. (Eds.), Bayesian Statistics. University Press, Valencia, Spain, pp. 143–203.

Brocher, T.M., 2005. Empirical relations between elastic wavespeeds and density in the Earth's crust. Bull. Seismol. Soc. Am. 95, 2081–2092.

Furumura, T., Koketsu, K., Wen, K.-L., 2002. Parallel PSM/FDM hybrid simulation of ground motions from the 1999 Chi-Chi, Taiwan, earthquake. Pure Appl. Geophys. 159, 2133–2146.

Hole, J., Zelt, B., 1995. 3-D finite-difference reflection traveltimes. Geophys. J. Int. 121, 427–434.

Hole, J., Clowes, R., Ellis, R., 1992. Interface inversion using broad side seismic refraction data and three-dimensional traveltime calculations. J. Geophys. Res. 97, 3417–3429.

Kinoshita, S., 1998. Kyoshin Net (K-NET). Seismol. Res. Lett. 69, 309–332.

Kohketsu, K., Shima, E., 1985. Q_P structure of sediments in the Kanto plain. Bull. Earthq. Res. Inst. Univ. Tokyo 60, 495–505.

Koketsu, K., Higashi, S., 1992. Three-dimensional topography of the sediment/basement interface in the Tokyo Metropolitan area, Central Japan. Bull. Seismol. Soc. Am. 82, 2328–2349.

Koketsu, K., Kikuchi, M., 2000. Propagation of seismic ground motion in the Kanto basin, Japan. Science 288, 1237–1239.

Komazawa, M., Hasegawa, I., 1988. The graven structure suggested by the gravimetric basement in the Kanto district, central Japan. Mem. Geol. Soc. Jpn. 31, 57–74 (in Japanese).

Magistrale, H., Day, S., Clayton, R., Graves, R., 2000. The SCEC southern California reference three-dimensional seismic velocity model version 2. Bull. Seismol. Soc. Am. 90, 565–576.

Miura, H., Midorikawa, S., 2001. Effects of 3-D deep underground structure on characteristics of rather long-period ground motion. Zisin 54, 381–395 (in Japanese with English abstract).

Nafe, J.E., Drake, C.L., 1963. Physical properties of marine sediments. The Sea, vol. 3. Interscience, New York, pp. 794–815.

Nishizawa, A., Kanazawa, T., Iwasaki, T., Shimamura, H., 1996. Crustal structure related to the Philippine Sea plate subduction in the northeastern part of the Sagami Trough, Japan. Phys. Earth Planet. Inter. 93, 21–36.

Olsen, K., Archuleta, R., Matarese, J., 1995. Three-dimensional simulation of a magnitude 7.75 earthquake on the San Andreas fault. Science 270, 1628–1632.

Paige, C., Saunders, M., 1982. LSQR: an algorithm for sparse linear equations and sparse least squares. Trans. Math. Softw. 8, 43–71.

Parsons, T., Blakely, R.J., Brocher, T.M., 2001. A simple algorithm for sequentially incorporating gravity observations in seismic traveltime tomography. Int. Geol. Rev. 43, 1073–1086.

Podvin, P., Lecomte, I., 1991. Finite difference computation of traveltimes in very contrasted velocity models: a massively parallel approach and its associated tools. Geophys. J. Int. 105, 271–284.

Sato, T., Graves, R., Somerville, P., 1999. Three-dimensional finite-difference simulation of long-period strong motions in the Tokyo Metropolitan area during the 1990 Odawara earthquake (M_J 5.1) and the great 1923 Kanto earthquake (M_S 8.2) in Japan. Bull. Seismol. Soc. Am. 89, 579–607.

Sato, H., Hirata, N., Koketsu, K., Okaya, D., Abe, S., Kobayashi, R., Matsubara, M., Iwasaki, T., Ito, T., Ikawa, T., Kawanaka, T., Kasahara, K., Harder, S., 2005. Earthquake source fault beneath Tokyo. Science 309, 462–464.

Sugiyama, Y., Sugai, T., Imura, R., Mizuno, K., Endo, H., Shimokawa, K., Yamazaki, H., 1997. 1:500,000 Neotectonic map, Sheet 8, Tokyo, 2 ed., Geological Survey of Japan.

Suzuki, H., 1996. Geology of the Koto deep borehole observatory and geological structure beneath the Metropolitan Area, Japan. Report of the National Research Institute for Earth Science and Disaster Prevention, vol. 56, pp. 77–123 (in Japanese with English abstract).

Suzuki, H., 1999. Deep geological structure and seismic activity in Tokyo Metropolitan area. J. Geogr. 108, 336–339 (in Japanese with English abstract).

Suzuki, H., Morino, M., Iwamoto, K., Liu, Y., Fujiwara, H., Hayakawa, Y., 2005. 3D subsurface structural model for strong motion simulation around Lake Biwa, southwest Japan. Zisin 58, 91–106 (in Japanese with English abstract).

Taira, A., Saito, S., Hashimoto, M., 1981. Fundamental process of building the Japanese islands. Kagaku 51, 508–515 (in Japanese with English abstract).

Talwani, M., 1973. Computer usage in the computation of gravity anomalies. 14 In: Bolt, B. (Ed.), Method in Computational Physics. Academic Press, New York, pp. 343–389.

Tondi, R., de Franco, R., Barzaghi, R., 2000. Sequential integrated inversion of refraction and wide-angle reflection traveltimes and gravity data for two-dimensional velocity structure. Geophys. J. Int. 141, 679–698.

Vidale, J., 1990. Finite-difference calculation of traveltimes in three dimensions. Geophysics 55, 521–526.

Vigneresse, J., 1977. Linear inverse problem in gravity profile interpretation. J. Geophys. 43, 193–213.

Yajima, T., 1981. Petrological characteristics and geological structure of the pre-Tertiary basement of Kanto plain. Mem. Geol. Soc. Jpn. 20, 187–206 (in Japanese).

Yamanaka, H., Yamada, N., 2002. Estimation of 3D S-wave velocity model of deep sedimentary layers in Kanto plain, Japan, using microtremor array measurements. Butsuri Tansa 55, 53–65 (in Japanese with English abstract).

Yamanaka, H., Seo, K., Midorikawa, S., Shima, E., Yanagisawa, M., 1988. On the seismic prospectings in the southwestern part of Tokyo metropolitan area. (3) Analyses of explosion data in 1983 and 1984. Zisin 41, 527–539 (in Japanese).

Yoshida, S., Koketsu, K., 1990. Simultaneous inversion of waveform and geodetic data for the rupture process of the 1984 Naganoken-Seibu, Japan, earthquake. Geophys. J. Int. 103, 355–362.

Zelt, C., Borton, P., 1998. Three dimensional seismic refraction tomography: a comparison of two methods applied to data from the Faeroe Basin. J. Geophys. Res. 103, 7187–7210.

Zelt, C., Smith, R., 1992. Seismic traveltime inversion for 2-D crustal velocity structure. Geophys. J. Int. 108, 16–34.